10-2007

Effect of Tip Resonances on Tunnelling Anisotropic Magnetoresistance in Ferromagnetic Break Junctions: A First-Principles Study

J. D. Burton
University of Nebraska at Lincoln, jdburton1@gmail.com

Renat F. Sabirianov
University of Nebraska at Omaha, rsabirianov@unomaha.edu

Julian P. Velev
University of Nebraska-Lincoln, jvelev2@unl.edu

Oleg N. Mryasov
Seagate Research, Pittsburgh, PA, omryasov@mint.ua.edu

Evgeny Y. Tsymbal
University of Nebraska at Lincoln, tsymbal@unl.edu

Effect of tip resonances on tunneling anisotropic magnetoresistance in ferromagnetic metal break-junctions: A first-principles study

J. D. Burton,[1,2,*,†] R. F. Sabirianov,[3,2] J. P. Velev,[1,2] O. N. Mryasov,[4] and E. Y. Tsymbal[1,2,*,‡]
[1]*Department of Physics and Astronomy, University of Nebraska, Lincoln, Nebraska 68588-0111, USA*
[2]*Nebraska Center for Materials and Nanoscience, University of Nebraska, Lincoln, Nebraska 68588-0111, USA*
[3]*Department of Physics, University of Nebraska, Omaha, Nebraska 68182-0266, USA*
[4]*Seagate Research, Pittsburgh, Pennsylvania 15222, USA*
(Received 10 October 2007; published 26 October 2007)

First-principles calculations of electron tunneling transport in nanoscale Ni and Co break-junctions reveal strong dependence of the conductance on the magnetization direction, an effect known as tunneling anisotropic magnetoresistance (TAMR). An important aspect of this phenomenon stems from resonant states localized in the electrodes near the junction break. The energy and broadening of these states is strongly affected by the magnetization orientation due to spin-orbit coupling, causing TAMR to be sensitive to bias voltage on a scale of a few millivolts. Our results bear a resemblance to recent experimental data and suggest that TAMR driven by resonant states is a general phenomenon typical for magnetic broken contacts. This effect may be observed in any experiment where a magnetic tip is used to probe electron transport, e.g., spin-polarized scanning-tunneling measurements.

DOI: 10.1103/PhysRevB.76.144430 PACS number(s): 75.47.−m, 72.15.Gd, 73.40.Gk, 73.63.−b

I. INTRODUCTION

Nanomagnetic materials are playing an increasingly important role in modern technologies spanning the range from information processing and storage to spin electronics (spintronics), communication devices, electrical power generation, and nanobiosensing.[1] In particular, magnetic-field control of electrical resistance in nanoscale ferromagnetic systems has been among the most promising avenues for spintronics applications.[2] For example, the resistance due to a narrow magnetic domain wall in nanowires, nanoconstrictions, and atomic-scale break-junctions has been examined extensively both theoretically and experimentally (for a review, see Ref. 3). Application of the magnetoresistance due to domain walls, however, has practical issues because the formation of a domain wall in any individual sample occurs, if at all, only for a very sample-specific range of magnetic-field magnitude.[4] Anisotropic magnetoresistance (AMR), on the other hand, is the difference in resistance of *any uniformly magnetized* ferromagnetic conductor as the magnetization direction is changed, by an applied field, with respect to the direction of current flow. AMR occurring in bulk ferromagnets originates from the anisotropy of scattering produced by spin-orbit coupling (SOC) in the diffusive transport regime.[5] The nature of AMR in nanoscale magnetic systems such as ballistic conductors or tunnel junctions is profoundly different due to the nondiffusive mechanisms that control electron transport. While the magnitude of AMR in these systems may vary from sample to sample, it will, in general, always be present and is sensitive to field magnitude only in that it must be enough to saturate the sample. This has led to a recent revival of interest in AMR phenomena on the nanoscale.

For example, it was found that in electrodeposited Co nanocontacts, the ballistic nature of electron transport leads to stepwise conductance changes as the angle of the magnetization is altered with respect to the axis of the wire.[6] A similar effect was observed in Fe break-junctions.[7] This phenomenon is known as ballistic anisotropic magnetoresistance.[8] Another kind of AMR is inherent to the tunneling transport regime and is called tunneling anisotropic magnetoresistance (TAMR). TAMR has been observed in tunnel junctions with dilute magnetic semiconductor electrodes.[9–12] It was also detected by scanning-tunneling spectroscopy of thin Fe films on W(110) substrates,[13] predicted for tunneling from metallic alloys with large magnetocrystalline anisotropy, such as CoPt,[14] and tunneling from the Fe(100) surface through vacuum.[15] TAMR was also recently observed in CoFe|MgO|CoFe and CoFe|Al_2O_3|CoFe magnetic tunnel junctions.[16] TAMR originates from the anisotropy of the electronic structure induced by SOC. It is different from the usual tunneling magnetoresistance (TMR) which is observed in magnetic tunnel junctions (for reviews on TMR, see Refs. 17 and 18). While TMR is due to the reorientation of magnetic moments of the two magnetic electrodes relative to one another, TAMR is intrinsic to magnetically saturated tunnel junctions and can even occur in junctions with only one magnetic electrode.[19]

Recently, Bolotin *et al.*[20] have shown that atomic-scale Permalloy break-junctions fabricated using electromigration techniques exhibit TAMR. By measuring the conductance of the completely broken contacts as a function of magnetic-field direction at saturation, Bolotin *et al.* found that the TAMR can be as large as 25%. They also found that magnetoresistance was sensitive to changes in bias on a scale of a few millivolts and exhibited a complex angular dependence. The origin of these phenomena was attributed to conductance fluctuations due to quantum interference effects based on a model proposed by Adam *et al.*[21] This model was, however, developed for *diffusive metallic* samples and, though it may be relevant to unbroken metallic junctions, it may not be applicable to tunneling conduction across broken contacts. Therefore, the origin of the large TAMR observed by Bolotin *et al.* and the source of its sensitivity to applied bias voltage remain elusive.

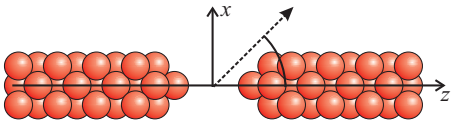

FIG. 1. (Color online) The atomic structure of the 5-4 break-junction. The z axis is the axis of the wire. The angle θ denotes the direction of the spin magnetic moments in the xz plane.

In this work, we present results of first-principles calculations of the electronic structure and conductance of Ni and Co break-junctions, where electron transport occurs via tunneling. We find a strong dependence of the tunneling conductance on the magnetization orientation, signature of the TAMR effect. We demonstrate the importance of resonant states localized at the electrode tips near the break, referred to as *tip resonances*, which are known to show up in atomically sharp transition metal tips.[22] The energy and broadening of these states depend strongly on the magnetization orientation due to the SOC. Our results at finite bias show sensitivity of TAMR on a scale of a few millivolts, and the angular dependence of TAMR bears a resemblance to the experimental results of Bolotin *et al.*,[20] indicating the origin of the observed phenomenon. We infer that TAMR driven by tip-resonant states is a general phenomenon typical for magnetic broken contacts and any other experimental geometry where a magnetic tip is used to probe electron transport.

II. METHOD

First, we consider Ni break-junctions consisting of two freestanding semi-infinite nanowire electrodes made of ferromagnetic fcc Ni which are separated by a vacuum region, as shown in Fig. 1. The nanowires are built along the [001] direction (z axis) by periodic repetition of a supercell made up of two topologically different (001) planes, one consisting of five atoms and the other of four atoms, which we designate as the 5-4 configuration. We use the lattice constant $a=3.52$ Å of bulk fcc Ni. The tip of each electrode has one apex atom, and the separation between the two apex atoms is equal to three atomic planes, or 5.28 Å.[23]

Self-consistent density functional calculations of the spin-dependent electronic structure of the Ni break-junctions are performed using the real-space recursion method[24] with a tight-binding linear muffin-tin-orbital (TB-LMTO) basis[25] in the atomic sphere approximation.[26] The local spin density approximation is used for the exchange-correlation energy. The SOC is included within a scalar relativistic approximation via perturbation for each atomic sphere. We assume that all atomic spheres have the same spin orientation, and the magnetization lies in the xz plane making an angle θ with respect to the z axis (Fig. 1). Therefore, the SOC term in the Hamiltonian is

$$\lambda \mathbf{L}\cdot\mathbf{S} = \frac{1}{2}\lambda[L_x(\sigma_z \sin\theta + \sigma_x \cos\theta) + L_y\sigma_y + L_z(\sigma_z \cos\theta - \sigma_x \sin\theta)], \quad (1)$$

where $\mathbf{L}$ and $\mathbf{S}$ are the orbital and spin momentum operators, respectively, $\boldsymbol{\sigma}$ is the Pauli spin matrix, and λ is the SOC constant.

To calculate transport properties of this break-junction, we appeal to the Landauer-Büttiker formalism of quantum transport[27] where the electric current is given by

$$I = \frac{e}{h}\int_{-\infty}^{\infty} T(E)[f(E-\mu_L) - f(E-\mu_R)]dE. \quad (2)$$

Here, $T(E)$ is the transmission probability for states with energy E, $f(E)$ is the Fermi distribution function, and μ_L (μ_R) is the electrochemical potential of the left (right) electrode.[28] The transmission function is given by

$$T(E) = \mathrm{Tr}[(\Sigma_L^\dagger - \Sigma_L)G(E)(\Sigma_R - \Sigma_R^\dagger)G^\dagger(E)], \quad (3)$$

where $G(E)$ is the retarded Green's function and Σ_L and Σ_R are the self-energies corresponding to the left and right electrodes, respectively. In the absence of applied bias, tight-binding techniques implemented within the TB-LMTO method can be used to calculate $T(E)$ directly from Eq. (3),[29] where the necessary real-space Hamiltonian blocks are taken from the fully self-consistent calculation. In general though, to evaluate the dependence on bias using Eq. (3), one needs to go beyond the equilibrium picture implicit in the first-principles calculations. To get a qualitative picture, however, we will use a simplified description in the spirit of the Bardeen approximation[30] in the low bias regime. This approach will be justified by comparing it with the full calculation method, Eq. (3), in the absence of applied bias.

If the coupling through vacuum is weak, then each electrode can be treated as an independent subsystem. Consider a tight-binding layer within the vacuum region of empty spheres in the plane $z=0$, and partition the left and right electrodes in Eq. (3) to include the metal electrodes and a portion of the vacuum up to that layer. If the layer lies in the vacuum at a sufficient distance from both metal surfaces, the self-energies Σ_L and Σ_R entering Eq. (3) can be treated as small. Retaining only terms of the order of Σ^2 in Eq. (3), we can replace the Green's function $G(E)$ of the coupled system evaluated at the layer by the Green's function of the uncoupled vacuum region $G_0(E)$. Within the same approximation, we can write the expression for the tunneling density of states (DOS) operator in the vacuum induced by the left and right electrodes, ρ_L and ρ_R, respectively, as follows:

$$2\pi i\rho_{L,R}(E) \approx G_0(E)(\Sigma_{L,R} - \Sigma_{L,R}^\dagger)G_0(E). \quad (4)$$

This allows us to rewrite Eq. (3) as

$$T(E) \approx 4\pi^2\,\mathrm{Tr}[G_0^{-1}(E)\rho_L(E)G_0^{-1}(E)\rho_R(E)], \quad (5)$$

where the trace is taken over all the orbital and spin indices over sites lying within the vacuum tight-binding layer. The transmission has been previously derived directly from the Bardeen approximation using the embedding Green's function approach.[31]

If only one orbital state dominates the conductance, which is typical for a not too thin vacuum barrier,[32] the expression for the transmission can be simplified further. Neglecting nondiagonal components of the DOS operator and the Green's function,[33] we find

$$T(E) \approx 4\pi^2\phi^2(E)[\rho_L^{\uparrow}(E)\rho_R^{\uparrow}(E) + \rho_L^{\downarrow}(E)\rho_R^{\downarrow}(E)], \qquad (6)$$

where $\rho_{L,R}^{\sigma}(E)$ is the tunneling DOS for spin projection σ along the magnetization axis, and $\phi(E)$ is the diagonal component of $G_0^{-1}(E)$ which has the meaning of an effective barrier potential seen by tunneling electrons. Equation (6) is reminiscent of the approximation used to derive Jullière's formula;[34] however, there is an important difference: Eq. (6) expresses the transmission in terms of the tunneling DOS in the *barrier*, while Jullière's formula is expressed in terms of the DOS of the *electrodes*.

In our case, the break-junction is symmetric and the tunneling DOS induced by the left and right electrodes are $\rho_L^{\sigma}(E)=\frac{1}{2}\rho^{\sigma}(E-eV)$ and $\rho_R^{\sigma}(E)=\frac{1}{2}\rho^{\sigma}(E)$, where V is an applied bias voltage and $\rho^{\sigma}(E)$ is the tunneling DOS induced by the *two* electrodes at *zero* bias. $\rho^{\sigma}(E)$ can be taken directly from one calculation of the fully coupled Green's function $G(E)$ in the absence of applied bias.

Application of this simplified approach is justified by calculating $T(E)$ using both Eqs. (3) and (6) in the absence of applied bias for energies near the Fermi level. Using an energy independent effective barrier height $\phi \approx 4$ eV, chosen by comparing the results, the calculations reveal excellent agreement between the two approaches for all orientations of the magnetization in the energy range considered [see Figs. 2(a), 2(d), and 2(g)].[35] Furthermore, for applied bias on the order of a few tens of millivolts, we can neglect the variation of ϕ with V, and therefore, Eq. (6) should provide a compelling qualitative picture of tunneling for the low bias regime.

III. RESULTS AND DISCUSSION

Figure 2(a) shows the transmission function calculated in the absence of SOC within ±30 meV of the Fermi energy (E_F). Comparing Fig. 2(a) to the band structure of the Ni electrode shown in Fig. 2(b), we see that at E_F, the features of the tunneling transmission are dominated by states on the apex atoms originating from a minority-spin d band [marked A in Fig. 2(b)]. This is evident from the distinctive drop at the bottom of the band in the local DOS at the apex atom [Fig. 2(c)] and in the transmission function [Fig. 2(a)]. Below the band minimum at −20 meV, there appear two narrow peaks in the transmission due to tip-resonant states [Fig. 2(a)].[36] These resonant states are seen in Fig. 2(c) and arise because the lower coordination of the apex atom reduces the effective on-site energy so that the level lies below the continuum of band A.[37] These tip-resonant states have minority d_{z^2} character, similar to the states of band A. The weak interaction through vacuum splits these states into a bonding-antibonding pair.[38] Another tip-resonant state at 12.8 meV [Figs. 2(a) and 2(c)] is double degenerate and is composed of the d_{xz} and d_{yz} orbitals. One more tip-resonant state barely visible in Fig. 2(a) at 23 meV is localized on the four atoms in the first subapex atomic layer [the dashed line in Fig. 2(c)].

Inclusion of SOC makes the nature of each tip-resonant state strongly dependent on the magnetization angle θ. The most important effect for the TAMR is the broadening of the d_{z^2} tip-resonant state [the bottommost resonance in Figs. 2(d), 2(f), 2(g), and 2(i)]. The broadening of this state is smaller for $\theta=0°$ because the SOC in Eq. (1) only mixes minority d_{z^2} states with majority d states and not with other minority d states.[39] However, when $\theta=90°$, the SOC mixes the minority d_{z^2} states with minority d_{xz} states resulting in significant broadening. In addition, the minority d band that has a maximum just below E_F [marked B in Figs. 2(b), 2(e), and 2(h)] at the Brillouin zone edge has significant d_{xz} character and the tip resonance can hybridize with this band, provided this band overlaps with the resonance level. Since the top of this band also varies with θ, only a certain range of θ will meet this condition, leading to the transition from the sharp double-peak feature of Figs. 2(d) and 2(f) to the broad resonance in Figs. 2(g) and 2(i).

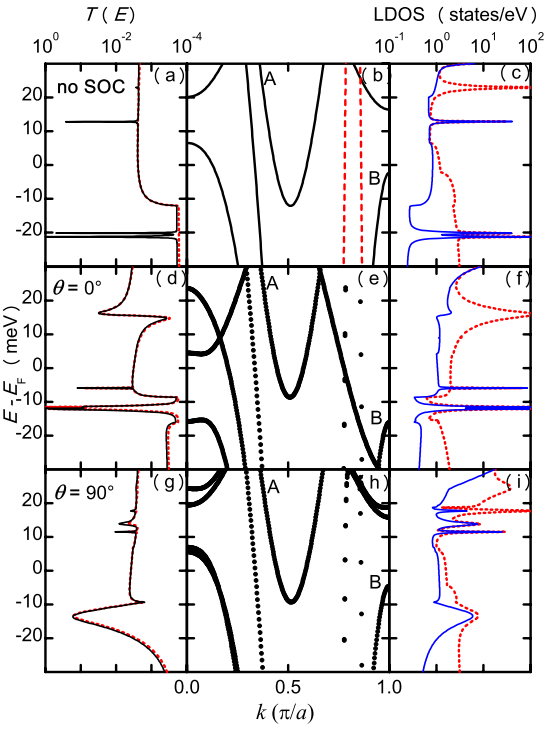

FIG. 2. (Color online) The transmission function, band structure of the electrodes, and the local DOS on the 5-4 electrode tips [(a)–(c)] without SOC and with SOC for [(d)–(f)] $\theta=0°$ and [(g)–(i)] $\theta=90°$. In (b), the solid curves are minority-spin bands, and the dashed curves are majority-spin bands. In (a), (d), and (g), the solid curves are calculated using Eq. (6) and the dashed curves are calculated using Eq. (3). In (c), (f), and (i), the solid curves are the minority DOS on the apex atom and the dashed curves are the minority DOS on the first subapex atomic layer.

Another effect of the SOC on the transmission function is the splitting of the d_{xz}, d_{yz} doublet [the peak at 12.8 meV in Figs. 2(a) and 2(c)] into two singlets. The splitting is largely determined by the $\frac{1}{2}\lambda L_z\sigma_z \cos\theta$ term in Eq. (1), making the splitting much stronger for $\theta=0°$ than for $\theta=90°$. For $\theta=0°$, the lower state of the split doublet is seen in Figs. 2(d) and 2(f) as a sharp peak at −6 meV. The upper state lies outside of the energy range plotted. For $\theta=90°$, the splitting is much weaker and occurs due to the coupling of the doublet states via other states (e.g., the bulk band A), producing two peaks at 11.8 and 17.4 meV, as seen in Figs. 2(g) and 2(i).

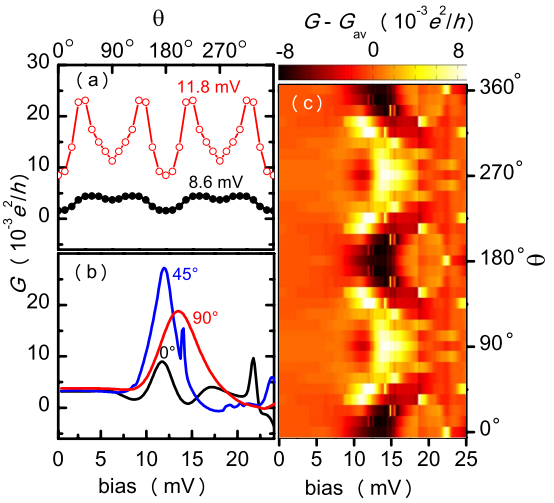

FIG. 3. (Color online) Variations of differential conductance $G(V)=dI/dV$ at 4.2 K for the 5-4 break-junction. (a) G versus θ for different bias voltages. (b) Dependence of G on bias for different θ. (c) Deviation of G from G_{av}, the conductance averaged over θ, as a function of V and θ.

One more feature induced by the SOC is the Fano-shaped resonance[40] seen in Fig. 2(d) at around 15 meV for $\theta=0°$. It mirrors a related feature that appears in the local DOS on the apex atom [Fig. 2(f)]. This resonance is due to the localized state that originates on the first subapex layer of atoms. In the absence of SOC, this state, appearing at 23 meV in Fig. 2(c), is not coupled to band A and does not appear in the DOS on the apex atom. However, when SOC is included, the state becomes coupled to band A and, by propagating through the band to the apex atom, acquires the Fano shape. For $\theta=90°$, the Fano resonance, appearing at 14 meV in Fig. 2(i), becomes less pronounced due to a weaker coupling between the resonant and continuum states.

The effect of bias is demonstrated in Fig. 3. Here, we plot the differential conductance $G(V)=dI/dV$ and its angular dependence. The current $I(V)$ is calculated using Eqs. (2) and (6), assuming the Fermi distribution function at a temperature of 4.2 K. As is evident from Fig. 3(a), the angular dependence of the conductance reflecting TAMR is very different from the $\cos(2\theta)$ dependence typical for bulk AMR.[5] The magnitude of TAMR is relatively large, e.g., it reaches 200% for $V=11.8$ mV. The conductance variation is quite sensitive to the applied bias, owing to the sensitivity of $\rho^{\sigma}(E)$ to θ due to resonant states. Figure 3(b) shows the bias dependence for a few values of θ. The central peak in Fig. 3(b) is due to the d_{z^2} tip resonance state which broadens with increasing angle from 0° to 90°. The Fano resonance can be seen between 14 and 16 mV for $\theta=0°$. Although finite temperature and bias smear out the sharp resonant features seen in Figs. 2(d) and 2(g), the angular dependence of the conductance is largely controlled by the tip-resonant states. Figure 3(c) shows the deviation of $G(V)$ from the value $G_{av}(V)$, the average over θ for applied bias V. Clearly, the deviation is strongly dependent on the bias voltage, and the central light-dark pattern is due to the variation of the d_{z^2} tip-resonant state with θ.

Figure 3(c) bears a resemblance to the plot of Fig. 4(d) of Bolotin *et al.*[20] Bolotin *et al.* attributed the variations observed in their experiments to conductance fluctuations due to quantum interference effects based on a model proposed by Adam *et al.*[21] This model was, however, developed for diffusive metallic samples and the application of this model to tunneling conduction across broken contacts is not clearly justified. The results presented here, however, indicate that the effect observed by Bolotin *et al.* may instead arise due to tip-resonant states, which are distinct from the quantum interference phenomena described by Adam *et al.*

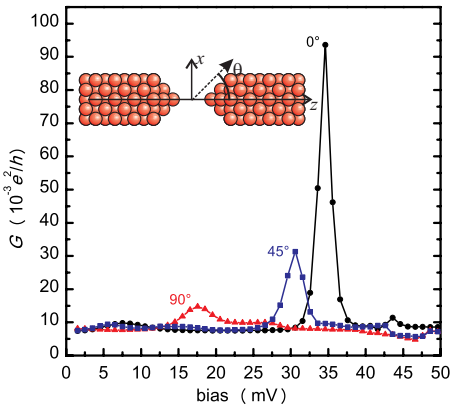

FIG. 4. (Color online) Differential conductance $G(V)=dI/dV$ at 4.2 K for the 13-12 break-junction (see inset) for three different magnetization orientations.

We also performed calculations for a Ni break-junction in a wire with larger radius. In this case, the two topologically different fcc (001) planes used to construct the electrodes consisted of 13 atoms in one plane and 12 atoms in the next, designated the 13-12 configuration. The pyramidal-apex tip structure and the separation of the two apex atoms were the same as in the 5-4 structure (see the inset of Fig. 4).

The bias dependent transport properties of the 13-12 junction are computed in the same way as the case of the narrow-wire break-junction. Transmission calculations for this structure using Eqs. (3) and (6) in the absence of applied bias reveal that an energy independent effective barrier height $\phi \approx 4.7$ eV produces excellent agreement between the two schemes for energies within ±50 meV of the Fermi level, indicating that Eq. (6) should again provide a reasonable qualitative picture of tunneling for biases below 50 mV.

The differential conductance $G(V)$ for the 13-12 break-junction is plotted in Fig. 4 for three orientations of the magnetization. The large peak at 35 mV for $\theta=0°$ derives from a resonant state, with minority d character, localized on the pyramidal-tip structure. The peak at 30 mV for $\theta=45°$ can also be attributed to this resonance, only shifted and broadened due to SOC.

The peak at 17 mV for $\theta=90°$ is also due to tip related electronic states with minority d character. This peak is related to the less pronounced and very broad variations in bias for the $\theta=0°$ and 45° orientations seen in the 5–20 mV range. While these features cannot be regarded as "resonant," they do arise from the inhomogeneous DOS on the tip and clearly lead to a nontrivial bias dependence of the TAMR effect.

We also examined a Co break-junction with the 5-4 structure, as in Fig. 1. Several tip-resonant states are present,

however, at different energies than those for the Ni 5-4 junction. In particular, a minority d_{z^2} tip resonance lies at ~100 meV above the Fermi energy and exhibits similar variation with θ as the one shown in Fig. 2. We therefore expect that tip-resonant states will be present in Co break-junctions and lead to similar bias dependent features of TAMR.

IV. CONCLUSIONS

In conclusion, based on first-principles calculations of the electronic structure and conductance of Ni and Co break-junctions, we have demonstrated that TAMR driven by tip-resonant states is a general phenomenon intrinsic to magnetic broken contacts. The energy and broadening of these states are strongly affected by the magnetization orientation, causing TAMR to be sensitive to bias voltage on a scale of a few millivolts. This explains the experimental results by Bolotin *et al.*[20] on TAMR in atomic-scale magnetic break-junctions.

We would like to emphasize the fact that the predicted phenomenon may occur in any geometry where a sharp magnetic tip is used to probe electron transport. In particular, the effect may be studied using a spin-polarized scanning-tunneling[41] setup where, contrary to the usual convention, a magnetic tip is used to scan a *nonmagnetic* surface. In this case, any observed TAMR effect would arise solely from the variation in the electronic structure of the tip, and tip-resonant features may be observed in the bias dependence. Tip resonances related to transition metal *d* states have already been observed in non-spin-polarized scanning-tunneling spectra using W tips.[22] We hope, therefore, that this work will stimulate further experimental studies of TAMR in magnetic tip geometries.

ACKNOWLEDGMENTS

We thank Dan Ralph and Kirill Belashchenko for helpful discussions. This work was supported by Seagate Research and jointly by the National Science Foundation and the Nanoelectronics Research Initiative through the Materials Research Science and Engineering Center (MRSEC) at the University of Nebraska.

*Corresponding author.
†jlz101@unlserve.unl.edu
‡tsymbal@unl.edu

[1] S. D. Bader, Rev. Mod. Phys. **78**, 1 (2006).
[2] I. Žutic, J. Fabian, and S. Das Sarma, Rev. Mod. Phys. **76**, 323 (2004).
[3] C. H. Marrows, Adv. Phys. **54**, 585 (2005).
[4] K. I. Bolotin, F. Kuemmeth, A. N. Pasupathy, and D. C. Ralph, Nano Lett. **6**, 123 (2006).
[5] J. Smit, Physica (Amsterdam) **17**, 612 (1951); T. R. McGuire and R. I. Potter, IEEE Trans. Magn. **11**, 1018 (1975).
[6] A. Sokolov, C. Zhang, E. Y. Tsymbal, J. Redepenning, and B. Doudin, Nat. Nanotechnol. **2**, 171 (2007).
[7] M. Viret, M. Gabureac, F. Ott, C. Fermon, C. Bareeteau, G. Autes, and R. Guiardo-Lopez, Eur. Phys. J. B **51**, 1 (2006).
[8] J. Velev, R. F. Sabirianov, S. S. Jaswal, and E. Y. Tsymbal, Phys. Rev. Lett. **94**, 127203 (2005).
[9] C. Gould, C. Rüster, T. Jungwirth, E. Girgis, G. M. Schott, R. Giraud, K. Brunner, G. Schmidt, and L. W. Molenkamp, Phys. Rev. Lett. **93**, 117203 (2004).
[10] C. Rüster, C. Gould, T. Jungwirth, J. Sinova, G. M. Schott, R. Giraud, K. Brunner, G. Schmidt, and L. W. Molenkamp, Phys. Rev. Lett. **94**, 027203 (2005).
[11] A. D. Giddings, M. N. Kahlid, T. Jungwirth, J. Wunderlich, S. Yasin, R. P. Campion, K. W. Edmonds, J. Sinova, K. Ito, K.-Y. Wang, D. Williams, B. L. Gallagher, and C. T. Foxon, Phys. Rev. Lett. **94**, 127202 (2005).
[12] H. Saito, S. Yuasa, and K. Ando, Phys. Rev. Lett. **95**, 086604 (2005).
[13] M. Bode, S. Heinze, A. Kubetzka, O. Pietzsch, X. Nie, G. Bihlmayer, S. Blügel, and R. Wiesendanger, Phys. Rev. Lett. **89**, 237205 (2002).
[14] A. B. Shick, F. Máca, J. Mašek, and T. Jungwirth, Phys. Rev. B **73**, 024418 (2006).
[15] A. N. Chantis, K. D. Belashchenko, E. Y. Tsymbal, and M. van Schilfgaarde, Phys. Rev. Lett. **98**, 046601 (2007).
[16] L. Gao, X. Jiang, S. Yang, J. D. Burton, E. Y. Tsymbal, and S. S. P. Parkin, Phys. Rev. Lett. (to be published).
[17] E. Y. Tsymbal, O. N. Mryasov, and P. R. LeClair, J. Phys.: Condens. Matter **15**, R109 (2003).
[18] E. Y. Tsymbal, in *Handbook of Magnetism and Advanced Magnetic Materials*, edited by H. Krohnmüller and S. S. P. Parkin (Wiley, Chichester, 2006), Vol. 5, pp. 2963–2978.
[19] J. Moser, A. Matos-Abiague, D. Schuh, W. Wegscheider, J. Fabian, and D. Weiss, Phys. Rev. Lett. **99**, 056601 (2007).
[20] K. Bolotin, F. Kuemmeth, and D. C. Ralph, Phys. Rev. Lett. **97**, 127202 (2006).
[21] S. Adam, M. Kindermann, S. Rahav, and P. W. Brouwer, Phys. Rev. B **73**, 212408 (2006).
[22] A. L. Vázquez de Parga, O. S. Hernán, R. Miranda, A. Levy Yeyati, N. Mingo, A. Martín-Rodero, and F. Flores, Phys. Rev. Lett. **80**, 357 (1998).
[23] Calculations with five and seven atomic plane separations between the apex atoms were also performed to check the general nature of the results. A larger separation only introduces an additional vacuum exponential decay in the transmission, therefore reducing the overall tunneling conductance. The qualitative picture of tip-resonant states affecting the TAMR is not altered.
[24] R. Haydock, *Solid State Physics* (Academic Press, New York, 1980), Vol. 35, pp. 215–294; O. Yu. Kontsevoi, O. N. Mryasov, A. I. Likhtenshtein, and V. A. Gubanov, Sov. Phys. Solid State **34**, 154 (1992).
[25] O. K. Andersen and O. Jepsen, Phys. Rev. Lett. **53**, 2571 (1984).
[26] Empty spheres fill the break-junction and surround the whole structure by three layers. All spheres, both Ni and empty, have the same radius and are arranged in an fcc structure.
[27] S. Datta, *Electronic Transport in Mesoscopic Systems* (Cambridge University Press, Cambridge, England, 1995).

[28] Here, T depends implicitly on applied bias $V=\mu_L-\mu_R$.
[29] R. F. Sabirianov, A. K. Solanki, J. D. Burton, S. S. Jaswal, and E. Y. Tsymbal, Phys. Rev. B **72**, 054443 (2005).
[30] J. Bardeen, Phys. Rev. Lett. **6**, 57 (1961).
[31] D. Wortmann, H. Ishida, and S. Blügel, Phys. Rev. B **72**, 235113 (2005).
[32] K. D. Belashchenko, E. Y. Tsymbal, M. van Schilfgaarde, D. A. Stewart, I. I. Oleynik, and S. S. Jaswal, Phys. Rev. B **69**, 174408 (2004).
[33] Nondiagonal components of the DOS operator and the Green's function with respect to atomic sites in the barrier contain a vacuum decay factor and therefore are small compared to diagonal components. Nondiagonal components of the DOS operator reflecting the spin-flip components of the conductance are normally small (see Ref. 15 for further discussion).
[34] M. Jullière, Phys. Lett. **54**, 225 (1975).
[35] In the absence of SOC, sharp peaks in the transmission due to localized states on the tip [Fig. 2(a)] appear in the Bardeen [Eq. (6)] but not in the Landauer-Büttiker [Eq. (3)] approach. This discrepancy, being a general feature of pure surface states (Ref. 31), becomes irrelevant in the presence of SOC which couples the tip-resonant states to the bulk states of the electrodes.
[36] To resolve the δ-function-like features of the tip states, a small imaginary part was added to the energy when plotting Figs. 2(a)–2(c).
[37] E. Y. Tsymbal and K. D. Belashchenko, J. Appl. Phys. **97**, 10C910 (2005).
[38] O. Wunnicke, N. Papanikolaou, R. Zeller, P. H. Dederichs, V. Drchal, and J. Kudrnovský, Phys. Rev. B **65**, 064425 (2002).
[39] Since $L_z|d_{z^2}\rangle=0$, the contribution from spin diagonal terms in Eq. (1) is zero. Due to the dominant s character, the majority-spin bands [the dashed lines in Fig. 2(b)] mix only very weakly with the minority d_{z^2} resonant states via SOC.
[40] U. Fano, Phys. Rev. **124**, 1866 (1961).
[41] M. Bode, Rep. Prog. Phys. **66**, 523 (2003).